Citation
Jin, H. and Hao, H. and Chen, W. and Xu, C. 2021. Effect of enhanced coating layer on the bandgap characteristics and response of metaconcrete. Mechanics of Advanced Materials and Structures. 30 (1): pp. 175-188. http://doi.org/10.1080/15376494.2021.2011498

Effect of enhanced coating layer on the bandgap characteristics and response of metaconcrete

Hexin Jin [a,b], Hong Hao [b*], Wensu Chen [b*], Cheng Xu [b]

[a] School of Civil Engineering, Tianjin University, Tianjin 300350, China

[b] Centre for Infrastructural Monitoring and Protection, School of Civil and Mechanical Engineering, Curtin University, Australia

[*]Corresponding authors: hong.hao@curtin.edu.au (H. Hao), wensu.chen@curtin.edu.au (W. Chen)

Abstract

Metaconcrete is made by partially or fully replacing natural coarse aggregates (NA) in normal concrete (NC) with engineered aggregates (EA). Normal engineered aggregate (NEA) is made by wrapping elastic coating outside spherical heavy core. It was found that mixing NEA in concrete could effectively mitigate stress wave propagation in metaconcrete structure owing to the local resonance of the heavy core of NEA. However, it also reduced the concrete material stiffness and strength because of the low modulus of soft coating that led to relatively large deformation of mortar matrix under loading. To address the issue of low interface stiffness while maintain the local vibration ability of NEA, new enhanced engineered aggregate (EEA) is proposed by placing an additional enhanced coating layer outside the soft coating of NEA. In this study, three types of EEA aggregates composed of three enhanced coating layer materials (i.e., epoxy resin, steel, ultra-high performance concrete UHPC) are considered and their configurations are designed via the software COMSOL. The spall behaviors of enhanced metaconcrete (EMC) mixed with EEA aggregates are examined though numerical simulations. 3D meso-scale models of EMC composed of mortar, randomly distributed natural aggregates and EEA aggregates are built via the software LS-DYNA. The distinction between the bandgap characteristics of NEA and EEA is studied. The effects of enhanced coating layer material on the bandgap of EEA and the performance of EMC with respect to energy absorption capacity, wave attenuation characteristics and spall strength are studied. The results show that the existence of enhanced coating layer slightly affects the bandgap characteristics of engineered aggregate. Applying an additional stiffer coating layer to make the EEA aggregates can improve the spall strength of metaconcrete mixed with EEA aggregates while its ability in mitigating

stress wave propagation and energy absorption is only slightly affected.

Keywords: Enhanced coating layer; Enhanced engineered aggregate; Metaconcrete; Bandgap; Spall damage; Meso-scale model;

Nomenclature

Engineered aggregate

NA	Natural aggregate
NEA-3.88	Normal engineered aggregate with central bandgap frequency of 3.88 kHz
NEA-7.64	Normal engineered aggregate with central bandgap frequency of 7.64 kHz
NEA-11.79	Normal engineered aggregate with central bandgap frequency of 11.79 kHz
EEA-steel-11.95	Enhanced engineered aggregate with an additional steel coating layer and central bandgap frequency of 11.95 kHz
EEA-epoxy-11.90	Enhanced engineered aggregate with an additional epoxy coating layer and central bandgap frequency of 11.91 kHz
EEA-UHPC-11.92	Enhanced engineered aggregate with an additional UHPC coating layer and central bandgap frequency of 11.92 kHz

Concrete structure

NC	Normal concrete structure
NMC	Normal metaconcrete structure composed of NEA aggregates with multiple bandgaps
EMC-epoxy	Enhanced metaconcrete structure composed of EEA-epoxy aggregates with multiple bandgaps
EMC-steel	Enhanced metaconcrete structure composed of EEA-steel aggregates with multiple bandgaps
EMC-UHPC	Enhanced metaconcrete structure composed of EEA-UHPC aggregates with multiple bandgaps

1. Introduction

Metamaterials with unique properties have drawn intensive research interests [1-6]. Zhang and Liu [7] demonstrated the negative refraction of acoustic waves in two-dimensional phononic crystals by introducing negative square root of the negative refraction index for acoustic waves. Fang et al. [8] made a new kind of metamaterial consisting of subwavelength

Helmholtz resonators. This kind of material had negative effective dynamic modulus near the resonance frequency of Helmholtz resonators, and could be used to make super lensing below the diffraction limit. On the other hand, by embedding metal cores coated with thin soft coating into epoxy matrix, Liu et al. [9] proposed locally resonant metamaterial. The effective mass of this material was frequency dependent and negative when the metal core moved out-of-phase with the epoxy resin matrix. The metal core coated with soft coating could stop the propagation of wave within the bandgap [10-13].

Metamaterials can be divided into Bragg-type metamaterial and locally resonant metamaterial [14]. For Bragg-type metamaterial, internal components need be distributed periodically. Huang and Shi [15] studied the dynamic response of structure behind two-dimensional periodic rows of piles under the action of periodic load. The results revealed that the bandgap (Bragg bandgap) was induced by the periodically distributed piles, and the vibration of structure behind periodic piles could be greatly reduced within the Bragg bandgap. However, the application of this type of metamaterial in civil engineering is limited [10]. For locally resonant metamaterial, the bandgap is generated by the resonance of heavy core, which does not require the periodic distribution [13, 16]. Hsu et al. [17] studied the propagation of Lamb wave in a two-dimensional locally resonant plate. The results showed that the propagation of Lamb wave with frequency corresponding to the bandgap of the locally resonant plate was attenuated. Cheng et al. [18] studied the dispersion relation and the possible engineering application of locally resonant metamaterial for low-frequency vibration isolation. The results showed that civil engineering structure based on the concept of local resonance could attenuate the damage caused by earthquake or vibration.

During service life, a structure might be subjected to blast and impact loads. Impulsive loading has the characteristics of high intensity and short duration. When an impulsive load is applied, compressive stress wave is generated and propagates in the structure. The compressive stress wave reflects and turns into tensile stress wave when it reaches the rear surface of the structure. Due to the superposition of the compressive and the reflected tensile stress waves at the rear of the structure, the structure might experience spalling damage. Metamaterial can be used to attenuate stress wave propagation induced by blast load. Mitchell et al. [10, 19, 20] numerically studied the response of NMC under blast load. The results showed that NEA aggregates could effectively attenuate the stress wave induced by blast load in NMC. Xu et al. [21] investigated the effects of geometric and material parameters of NEA on the frequency region of stress wave attenuated in NMC. Jin et al. [22] analytically investigated the performance of NMC in attenuating blast-induced stress wave. The results showed that the heavy core could partially dissipate the energy induced by blast load in NMC because of the relative movement between heavy core and matrix. Jin et al. [23] established a 3D meso-scale model of NMC, and studied the effects of volume fraction of NEA, elastic modulus and thickness of soft coating on the spall behaviors of NMC. It was reported that the energy absorption ability of NMC was affected by the volume fraction of NEA, the elastic modulus and thickness of soft coating. Jin et al. [24] proposed a procedure to properly design the engineered aggregates to have their bandgaps coinciding with the targeted predominant wave frequencies of stress wave in NC specimen, and demonstrated using the properly designed NEA can lead to more effective stress wave attenuation in metaconcrete via 3D meso-scale modelling.

Spall test is an effective experimental method to estimate the dynamic tensile strength of brittle materials [25-28]. This experimental technique does not require the stress equilibrium condition which is often not easy to achieve in a wide range of strain rates [29]. Wu et al. [26] experimentally investigated the dynamic tensile strength of concrete by spall test. Chen et al. [25] built a 3D meso-scale model to simulate the spall behaviors of concrete via the software LS-DYNA, and studied the effect of aggregate on the response of concrete in spall test. Empirical equations were proposed to predict the attenuation of stress wave propagation in concrete. Jin et al. [24] also built a 3D meso-scale model of metaconcrete composed of NEA aggregates to study the spall behaviors of the metaconcrete material.

This study extends the previous work reported by the authors [24]. The latter study found that although the stress wave amplitudes were reduced owing to the wave propagation mitigation effect by NEA in metaconcrete material, the spalling damage was not necessarily less severe compared to NC without NEA because mixing NEA reduced the concrete strength. This is because the soft coating of NEA can induce relatively larger deformation, which causes damage to brittle mortar matrix of the concrete hence reduces the concrete strength. To mitigate this shortcoming of the current designs of engineered aggregates, improved designs of NEA are proposed in this study by placing an additional stiff coating layer on NEA. Numerical study is carried out to evaluate the effectiveness of the new design of engineered aggregates with different types of additional coating layer on metaconcrete strength and mitigation of stress wave propagation. Based on the predominant frequency of stress wave propagation in NC specimen within elastic range, EEA made of heavy core, soft coating and enhanced coating layer is designed via the software COMSOL. The EEA aggregates respectively made with three enhanced coating layer materials (i.e., epoxy resin, steel, UHPC) are considered. To study the response of EMC in spall test, a 3D meso-scale model of EMC specimen considering aggregates with random size and distribution is built in the software LS-DYNA. The effects of enhanced coating layer material on the bandgap characteristics of EEA, the energy absorption capacity and the spall strength of EMC are studied to demonstrate the effectiveness of possible designs of EEA for practical application to producing metaconcrete materials.

2. Numerical model of enhanced metaconcrete specimen

2.1. 3D meso-scale model

Concrete is a heterogeneous material mainly composed of mortar and coarse aggregates. Numerical model in meso-scale (mm scale) can be established by distinctively modelling the different components in concrete to account for its heterogeneity and material properties. Meso-scale models of concrete have been used in many previous studies, e.g. [25, 27]. In this study, a 3D meso-scale model is generated for the metaconcrete with randomly distributed natural and engineered aggregates. Fig. 1 shows 3D meso-scale model of EMC specimen with 74 mm diameter and 500 mm length [25-27]. The EMC specimen is composed of mortar, NA aggregates and EEA aggregates. In the numerical model, the volume fraction of aggregates is 30%, and the aggregates are divided into three grades based on the Fuller's curve [30], i.e., 8-12 mm, 12-16 mm and 16-20 mm. The third-grade aggregates (i.e., 16-20 mm) consist of 70% NA and 30% EEA. The volume percentage of EEA aggregates accounts for 2.59% of the total specimen volume. In this study, both the thicknesses of soft coating and enhanced coating layer remain unchanged as 2 mm. All components in the specimen are simulated by the constant stress solid element. Mesh convergence test and model calibration have been conducted and reported in Jin et al. [23, 24], which is not repeated here. The mesh size of 0.5 mm after conducting mesh convergence test is determined and used in this study [23, 24]. The contact between different components is assumed as perfectly bonded. For comparison, the meso-scale models of NMC specimen and NC specimen are also established in this study. The NMC specimen model is established by replacing the enhanced coating layer of EEA aggregates in EMC specimen with mortar material. Similarly, the NC specimen model is established by replacing the whole EEA aggregates in EMC specimen with natural aggregates.

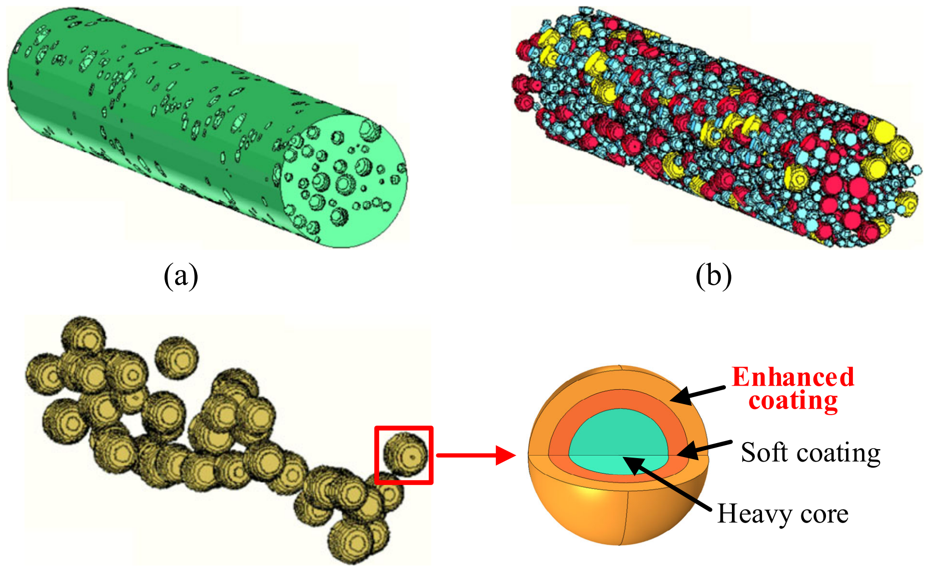

(c)

Fig. 1 3D meso-scale model of EMC specimen, (a) Mortar matrix, (b) Aggregates, (c) EEA aggregates with enhanced coating layer

2.2. Material model and strain rate effect

In this study, heavy core and soft coating are made of magnetite and polyurethane, respectively, which are assumed as linear elastic material in numerical model. Three kinds of materials (i.e., epoxy resin, steel, UHPC) are selected for the enhanced coating layer. Both epoxy resin and steel are also assumed as linear elastic in numerical simulations. Mortar, natural aggregate and UHPC are modelled by the KCC model (MAT_072R3) in LS-DYNA, which is widely used in the modelling of concrete-like material. Material parameters of different components in EMC specimen are given in Table 1. The parameters of the KCC model are generated based on the unconfined compressive strength of the material [31]. The strength surface parameters in KCC model are modified to simulate UHPC material as given in Table 2. The maximum principal strain of 0.1 is used as erosion criterion for mortar, natural aggregate and UHPC.

Table 1 Material parameters of different components in EMC specimen [9, 25, 32, 33]

Material	Density (kg/m^3)	Elastic modulus (GPa)	Compressive strength (MPa)	Poisson's ratio
Mortar	2100	--	34	0.19
UHPC	2470	--	125	0.23
Natural aggregate	2600	--	160	0.16
Magnetite	5200	68	--	0.17
Epoxy resin	1900	35	--	0.15
Steel	7800	200	--	0.10

Noted: "--" means the value is not required for the respective material model in LS-DYNA.

Table 2 Strength surface parameters modified in the KCC model for UHPC [34]

Material	a_0	a_1	a_2	a_{1f}	a_{2f}	a_{0y}	a_{1y}	a_{2y}
UHPC	2.407×10^{7}	0.36	1.26×10^{-9}	0.42	8.19×10^{-10}	1.316×10^{7}	0.23	4.29×10^{-9}

The strain rate effect on the strength of mortar, natural aggregate and UHPC is considered in the simulation. The dynamic increase factors for the dynamic compressive (DIF_c) and tensile (DIF_t) strength of mortar, natural aggregate and UHPC are defined by Eqs. (1)-(6).

The DIFs for mortar strength [12, 35, 36],

$$DIF_c=\begin{cases}0.0419(\log\dot{\varepsilon}_d)+1.2165 & \text{For } \dot{\varepsilon}_d<30\text{s}^{-1}\\ 0.8988(\log\dot{\varepsilon}_d)^2\text{-}2.8255(\log\dot{\varepsilon}_d)+3.4907 & \text{For } 30\text{s}^{-1}\le\dot{\varepsilon}_d\le1000\text{s}^{-1}\end{cases}\tag{1}$$

$$DIF_t=\begin{cases}(\dot{\varepsilon}_d/\dot{\varepsilon}_{ts1})^{\delta} & \text{For } \dot{\varepsilon}_d\le1\text{s}^{-1}\\ \beta(\dot{\varepsilon}_d/\dot{\varepsilon}_{ts1})^{1/3} & \text{For } \dot{\varepsilon}_d>1\text{s}^{-1}\end{cases}\tag{2}$$

where $\delta=1/(1+8f_{cs}/f_{c0})$, $\log\beta=6\delta-2$, $f_{c0}=10\text{MPa}$, $\dot{\varepsilon}_{ts1}=10^{-6}\text{s}^{-1}$ is the quasi-static strain rate for mortar, f_{cs} is the quasi-static compressive strength.

The DIFs for natural aggregate strength [37],

$$DIF_c=\begin{cases}0.0187(\log\dot{\varepsilon}_d)+1.2919 & \text{For } 1\text{s}^{-1}\le\dot{\varepsilon}_d<220\text{s}^{-1}\\ 1.8547(\log\dot{\varepsilon}_d)^2\text{-}7.9014(\log\dot{\varepsilon}_d)+9.6674 & \text{For } 220\text{s}^{-1}\le\dot{\varepsilon}_d\le1000\text{s}^{-1}\end{cases}\tag{3}$$

$$DIF_t=\begin{cases}0.0598(\log\dot{\varepsilon}_d)+1.3588 & \text{For } 10^{-6}\text{s}^{-1}\le\dot{\varepsilon}_d<0.1\text{s}^{-1}\\ 0.5605(\log\dot{\varepsilon}_d)^2+1.3871(\log\dot{\varepsilon}_d)+2.1256 & \text{For } 0.1\text{s}^{-1}\le\dot{\varepsilon}_d\le50\text{s}^{-1}\end{cases}\tag{4}$$

where the DIF_t of natural aggregate is taken as constant when strain rate exceeds 50 s^{-1} [25].

The DIFs for UHPC strength [38, 39],

$$\mathrm{DIF_c}=\begin{cases}(\dot{\varepsilon}_d/\dot{\varepsilon}_{ts2})^{0.014} & \text{For } \dot{\varepsilon}_d \le 62\mathrm{s}^{-1} \\ 0.587(\log\dot{\varepsilon}_d)^2\text{-}1.435(\log\dot{\varepsilon}_d)+1.911 & \text{For } \dot{\varepsilon}_d > 62\mathrm{s}^{-1}\end{cases} \quad (5)$$

$$\mathrm{DIF_t}=\begin{cases}(\dot{\varepsilon}_d/\dot{\varepsilon}_{ts2})^{0.018} & \text{For } \dot{\varepsilon}_d \le 10.3\mathrm{s}^{-1} \\ 9.959(\log\dot{\varepsilon}_d)\text{-}8.718 & \text{For } \dot{\varepsilon}_d > 10.3\mathrm{s}^{-1}\end{cases} \quad (6)$$

where $\dot{\varepsilon}_{ts2}=30\times10^{-6}\mathrm{s}^{-1}$ is the quasi-static strain rate for UHPC material.

3. Effect of enhanced coating layer on the bandgap characteristics of engineered aggregate

3.1. Determination of predominant wave frequencies of NC specimen in spall test

In this section, the response of NC specimen subjected to a small impulsive load within elastic range is calculated to determine the predominant wave frequencies of stress waves propagating in the specimen for the design of EEA so that the bandgaps of EEA aggregates coincide with those predominant wave frequencies [24]. Fig. 2 shows the numerical model of NC specimen in this study. A cross-section CS at 100 mm from the free end of the specimen and a mortar element E1 on the specimen periphery surface as shown in Fig. 2 are selected to extract the stress wave in NC specimen. The impulsive load with 6 MPa amplitude and duration of 0.1 ms as shown in Fig. 3 is applied onto NC specimen [25, 27].

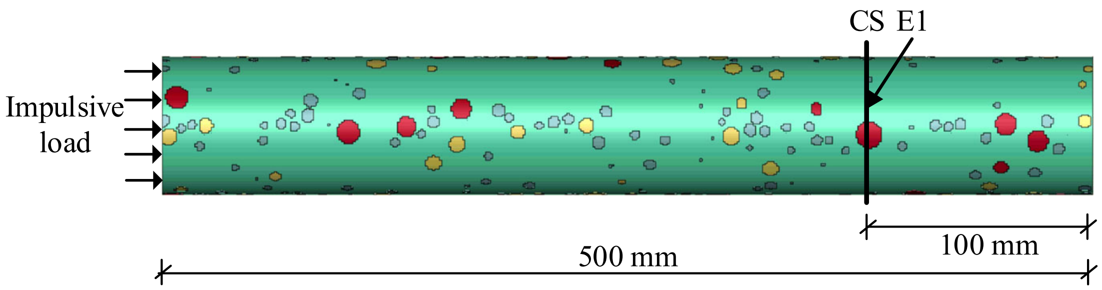

Fig. 2 Schematic diagram of CS and E1 (CS: cross-section and E1: mortar element)

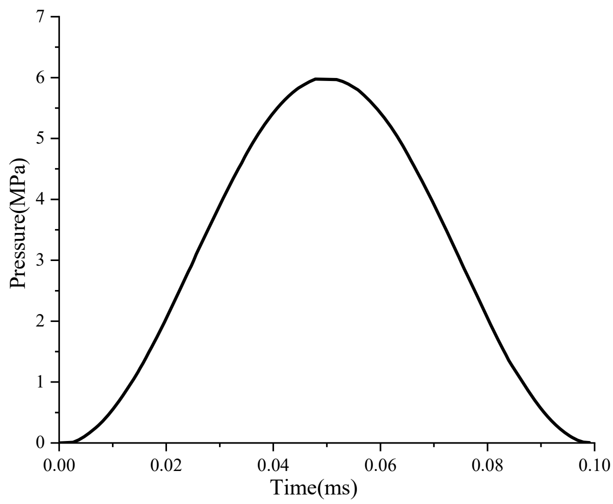

Fig. 3 Impulsive load with 6 MPa amplitude and 0.1 ms duration [25, 27]

Fig. 4(a) and (b) show the stress time histories of NC specimen at CS and E1 in the time domain and frequency domain, respectively. The stress over the cross section CS is the average stress of the whole cross-section area. As shown in Fig. 4(a), the stress time histories at CS and E1 are very close, which indicates the response at E1 can represent the response at the cross section CS. Fig. 4(b) shows the FFT spectrum of the stress wave. As shown, there are three amplitudes at 3.92 kHz, 7.84 kHz and 11.80 kHz in the frequency domain, indicating the wave energy concentrates at these three frequencies.

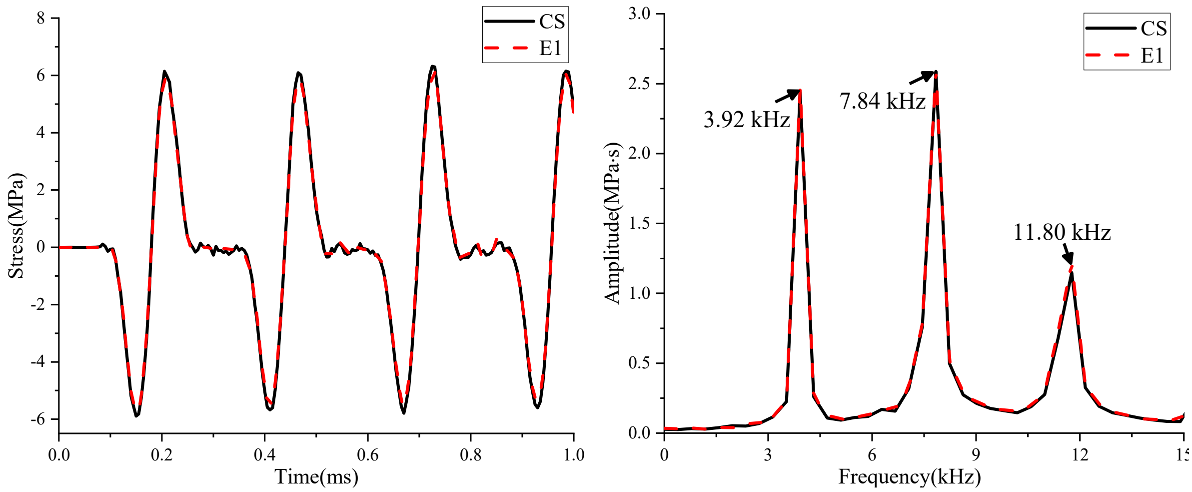

(a) (b)

Fig. 4 Stress time histories at CS and E1, (a) Time domain, (b) Frequency domain

3.2. Effect of enhanced coating layer on the bandgap of engineered aggregate

To achieve the best wave attenuation effect, the engineered aggregate should be designed to have the bandgap covering the predominant frequency of wave energy [24]. In this study, EEA is designed based on the predominant frequencies of stress wave propagating in NC specimen. As shown in Fig. 4(b), the wave energy concentrates around three frequencies, namely 3.92 kHz, 7.84 kHz and 11.80 kHz. Therefore, three types of EEA aggregates need be designed corresponding to these three frequencies.

As demonstrated in [21, 24], the bandgap of engineered aggregate can be adjusted by varying the material properties and dimensions of heavy core and soft coating. In this study, the NA aggregates that are replaced by engineered aggregates have diameter varying from 16 mm to 20 mm as described above. Therefore, the size of EEA also keeps in this range to be consistent with the size of NA. To simplify the analysis, the average diameter of 18 mm is used in the design analysis of EEA. Furthermore, as mentioned above, without loss of generality, both the thicknesses of soft coating and enhanced coating layer are set as 2 mm in this study, and magnetite is used as the core, which has rather fixed material properties. Therefore, to design the engineered aggregate for the bandgap covering the predominant wave frequency, the only parameter that can be varied is the elastic modulus of polyurethane coating. It is known that the elastic modulus of polyurethane varies in a large range from 0.5 MPa to 1000 MPa [40]. In this study, the software COMSOL is used to calculate the bandgaps of 18 mm-diameter engineered aggregates with 10 mm magnetite core, 2 mm-thick enhanced coating layer and 2 mm-thick polyurethane coatings with different elastic modulus. The polyurethane coatings designed for 18 mm-diameter EEA aggregates with the desired bandgap are then used for EEA aggregates to replace the natural aggregates with the diameter ranging from 16 mm to 20 mm.

Table 3 gives the material parameters of polyurethane coatings designed for EEA aggregates with diameter altered from 16 mm to 20 mm and NEA aggregates with diameter altered from 12 mm to 16 mm. Table 4 gives the bandgap characteristics (frequency range and width) of these EEA aggregates. The bandgap characteristics of NEA aggregates with diameter altered from 12 mm to 16 mm and the desired bandgaps reported in [24] are also given in Table 4 for comparison. It should be noted that EEA is made by adding a 2 mm additional enhanced coating layer to the NEA, therefore the 12 mm to 16 mm diameter NEA aggregates correspond to the 16 to 20 mm EEA aggregates without the external enhanced coating layer. It is found that the variation of the engineered aggregate size and enhanced coating layer material slightly changes the bandgap characteristics of EEA. For instance, the central bandgap frequency of EEA-steel-11.95 is 150 Hz higher than the desired central bandgap frequency of 11.80 kHz as shown in Fig. 4(b). Comparing the bandgap characteristics of EEA aggregates and NEA aggregates given in Table 4, the elastic modulus of polyurethane coating (69.00 MPa) designed for EEA-steel-11.95 is slightly higher than that (67.60 MPa) for EEA-epoxy-11.90 and that (65.00 MPa) for NEA-11.79. The bandgap width (3.11 kHz) of EEA-steel-11.95 is slightly narrower than the corresponding one of EEA-epoxy-11.90 (3.27 kHz), EEA-UHPC-11.92 (3.28 kHz) and NEA-11.79 (3.43 kHz). Nonetheless, these results demonstrate that adding an external enhanced coating layer on NEA only slightly changes the bandgap properties designed based on NEA configuration, and the bandgap of EEA can be designed to cover the predominant frequency of wave propagation.

Table 3 Material parameters of polyurethane coating designed for different engineered aggregates [24, 40]

Engineered aggregate	Density of polyurethane (kg/m^3)	Poisson's ratio of polyurethane	Elastic modulus of polyurethane (MPa)
EEA-UHPC-3.96	900	0.39	7.43
EEA-UHPC-7.92			29.80
EEA-UHPC-11.92			67.90
EEA-epoxy-3.96			7.42
EEA-epoxy-7.91			29.70
EEA-epoxy-11.90			67.60
EEA-steel-3.97			7.58
EEA-steel-7.94			30.40
EEA-steel-11.95			69.00
NEA-3.88			7.00
NEA-7.64			27.80
NEA-11.79			65.00

Table 4 Bandgap characteristics of engineered aggregates [24]

Engineered aggregate	Diameter range (mm)	Bandgap frequency range (kHz)	Bandgap width (kHz)
EEA-UHPC-3.96	16-20	3.42-4.50	1.08
EEA-UHPC-7.92		6.83-9.00	2.17
EEA-UHPC-11.92		10.28-13.56	3.28
EEA-epoxy-3.96		3.42-4.49	1.07
EEA-epoxy-7.91		6.83-8.99	2.16
EEA-epoxy-11.90		10.26-13.53	3.27
EEA-steel-3.97		3.45-4.48	1.03
EEA-steel-7.94		6.91-8.97	2.06
EEA-steel-11.95		10.39-13.50	3.11
NEA-3.88	12-16	3.32-4.44	1.12
NEA-7.64		6.91-8.97	2.07
NEA-11.79		10.07-13.50	3.43

4. Response of EMC specimen in spall test

4.1. Response of EMC specimen in spall test in elastic range

In order to study the effect of enhanced coating layer on the energy absorption ability of engineered aggregate, the elastic responses of EMC specimen composed of EEA aggregates with the same enhanced coating layer and multiple bandgaps are studied first. The impulsive load as shown in Fig. 3 is applied to EMC specimen. A magnetite element E2 and a mortar element E3 at cross-section CS as shown in Fig. 5 are selected to study the displacement response of EMC specimen. Responses of NC and NMC specimens are also simulated for comparison. To study the mechanism of EEA bandgap for EMC specimen, the strain of a polyurethane element E4 at cross-section CS of EMC and NMC as shown in Fig. 5 is analyzed. It should be noted since only elastic response is considered, the energy absorption and wave mitigation can be attributed primarily to the effect of engineered aggregates.

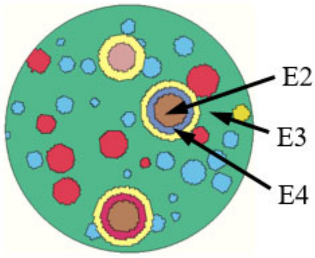

Fig. 5 Schematic diagram of E2-E4

(E2: magnetite element; E3: mortar element; E4: polyurethane element)

Fig. 6(a)-(e) show the displacement time histories of E2 and E3 for NC, NMC and different EMC specimens, respectively. Because of the relatively low stiffness of polyurethane coating, there is relative movement between magnetite core and mortar matrix for metaconcrete specimens, and no relative movement is observed in NC specimen as there is no polyurethane coating. As shown in Fig. 6(c)-(e), even though EEA is made by adding additional enhanced coating layer with higher stiffness outside NEA, there is still relative movement between magnetite core and mortar matrix for EMC specimen due to polyurethane coating. Fig. 7(a)-(d) show the time histories of kinetic energy and potential energy absorbed by different components in NMC and EMC specimens, respectively. As shown, because of the relative movement between magnetite core and mortar matrix, EEA aggregates, like NEA, absorb the energy induced by the impulsive load in EMC specimen through local heavy core vibrations. The ratio of the maximum energy absorbed by engineered aggregates to the total energy is 63.73% (NMC), 57.23% (EMC-epoxy), 56.74% (EMC-steel) and 58.43% (EMC-UHPC), respectively. The energy absorbed by EEA is slightly less than that by NEA because the heavy core vibration is less excited owing to the existence of the external relatively stiff coating layer. Larger impulsive loading would induce larger heavy core vibrations, then more energy absorptions by EEA is expected if impact load is larger. Large impulsive loading could damage mortar matrix, which also absorbs energy imparted into the specimen. Here only the energy absorption capacity of the engineered aggregate is discussed.

These results demonstrate that placing additional enhanced coating layer outside soft coating slightly reduces the energy absorption capacity of engineered aggregate in metaconcrete as compared to using NEA. These observations can also be explained by the bandgap properties of EEA and NEA. As presented above, placing an external stiff coating layer on NEA slightly shifts the central frequency of the bandgap and narrows the bandgap width, which make the EEA less effective in mitigating stress wave propagation than NEA. For instance, the central bandgap frequency of EEA-UHPC-11.92 is 11.92 kHz, while that of the NEA-11.79 is 11.79 kHz. As shown in Fig. 4, the third band of wave energy concentrates around 11.80 kHz, very close to the central bandgap frequency of NEA-11.79, resulting in the NEA-11.79 more effective in mitigating propagation of the stress wave than EEA-UHPC-11.92. It should be noted that by adjusting the EEA designs, its bandgap central frequency can be made to coincide with the desired frequency. However, this is not made here for comparison and discussion of the influences of adding an enhanced external coating layer on NEA on the bandgap properties. Nonetheless, as discussed above, adding an external stiff coating layer only slightly changes the bandgap properties, and the EEA is still effective in absorbing wave energy and mitigating stress wave propagation in metaconcrete. The above results also indicate that the energy dissipation by engineered aggregate mainly comes from the kinetic energy of heavy core and the potential energy of soft coating [22]. Therefore, using different enhanced coating layers has a very limited influence on the energy absorption capacity of metaconcrete.

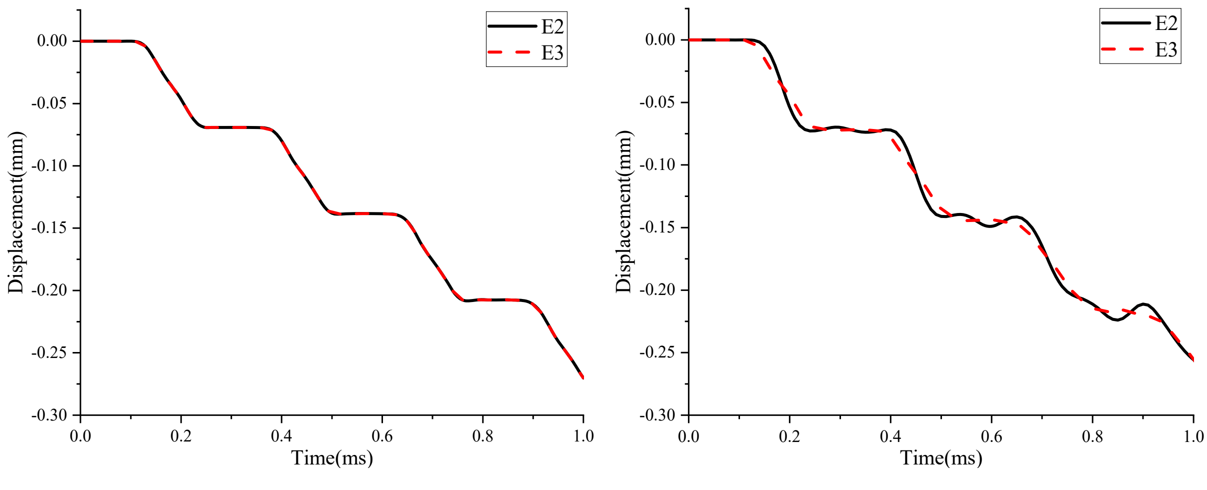

(a) (b)

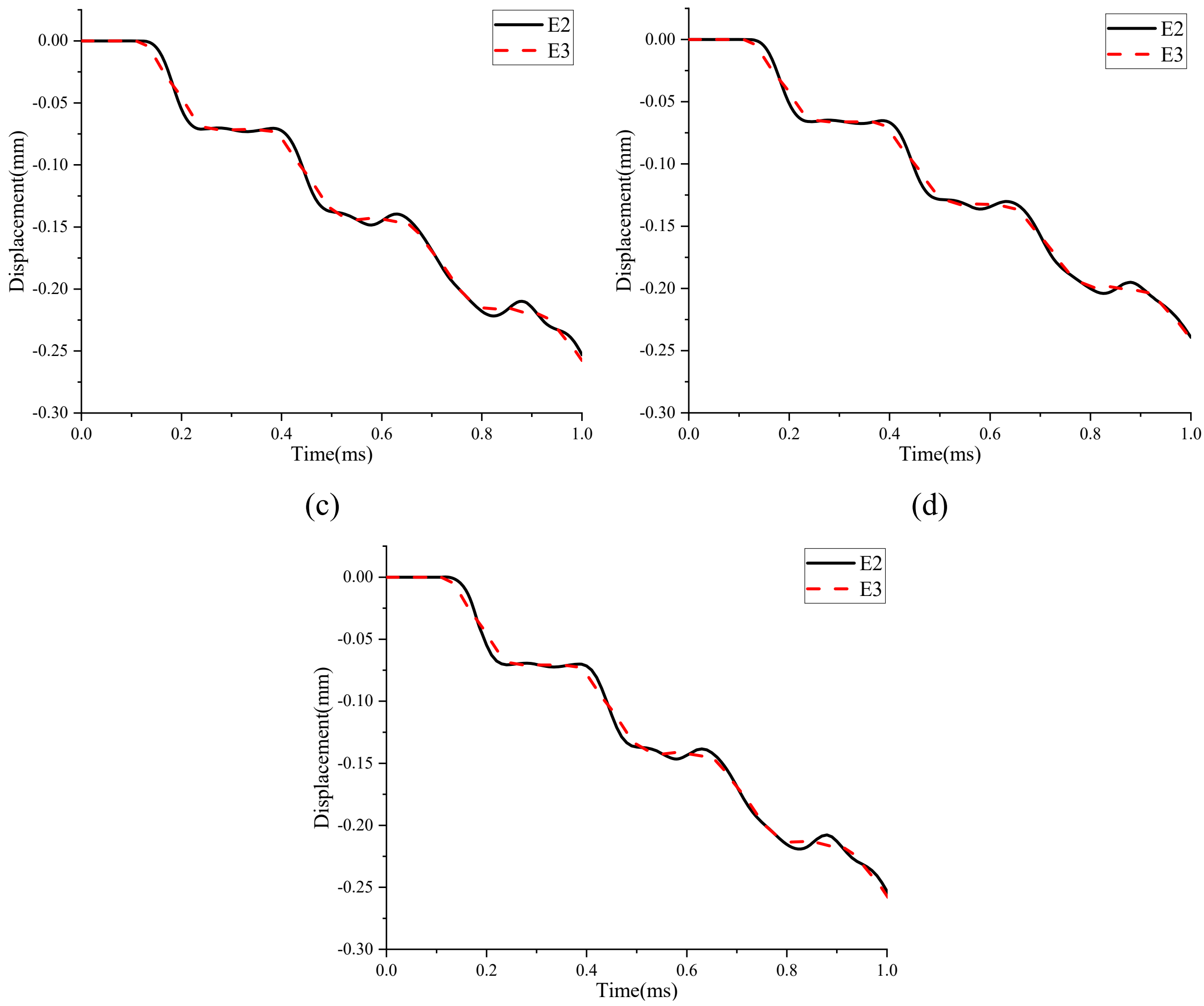

(c) (d)

(e)

Fig. 6 Displacement time histories of E2 and E3, (a) NC specimen,(b) NMC specimen, (c) EMC-epoxy specimen, (d) EMC-steel specimen, (e) EMC-UHPC specimen

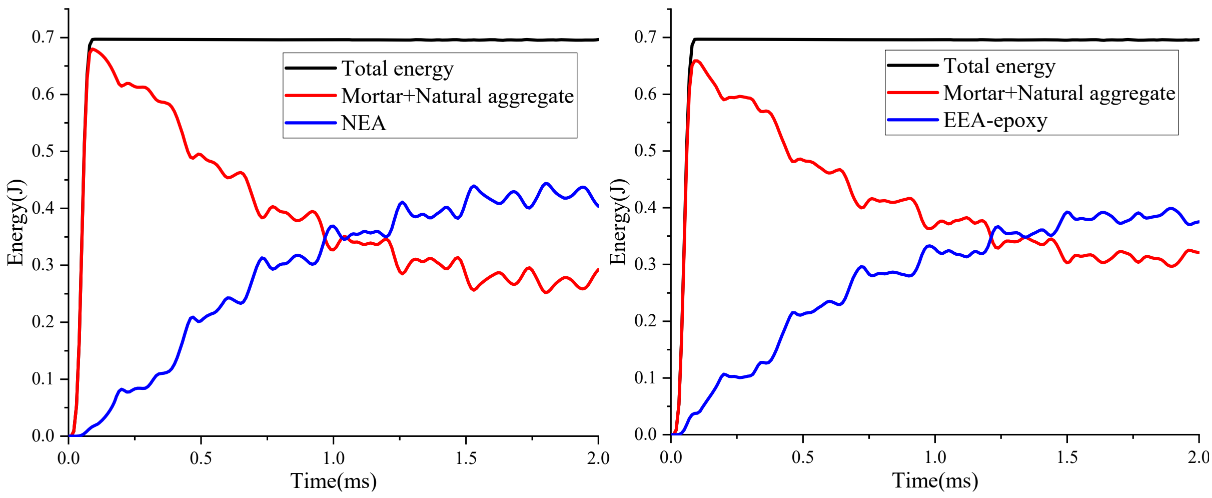

(a) (b)

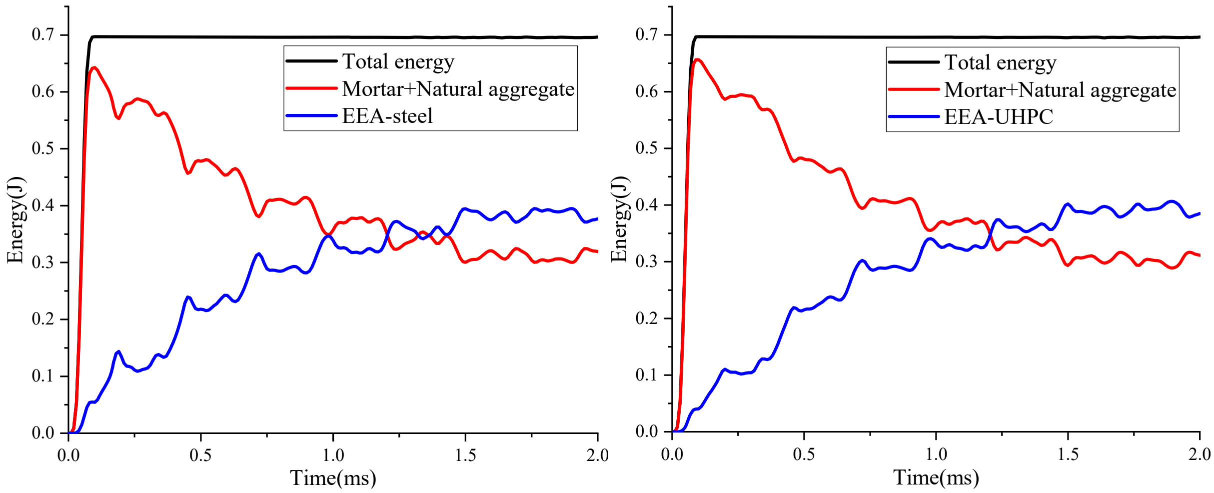

(c) (d)

Fig. 7 Time histories of energy absorption, (a) NMC specimen, (b) EMC-epoxy specimen, (c) EMC-steel specimen, (d) EMC-UHPC specimen

To further examine the mechanism of energy absorption of EEA, the stress wave propagations in EEA and NEA are analytically studied. Fig. 8(a) and (b) show the analytical model of NEA and EEA, respectively, in which H* represents heavy core, S* represents soft coating, E* represents enhanced coating layer and M* represents mortar matrix. As shown in Fig. 8(c), along the radial direction of EEA, a cylinder with diameter *d* is selected for analytical derivation. Analytical model of part of EEA is applied with free boundary condition. The contact between different materials is assumed as perfect bonding. All materials of EEA and NEA are assumed as elastic and isotropic in the analytical model. Material damping is neglected in the analytical derivation for simplicity as damping is normally neglected in estimating structural response to short-duration impulsive loads. The incident stress wave σ_I propagates from mortar to enhanced coating layer. Assuming the arc length *l* as shown in Fig. 8(c) is approximately equal to *d*, which means the stress wave in the analytical model can be assumed as one-dimensional stress wave. When the elastic wave reaches the interface between two materials with different impedances, the incident stress wave is partially reflected and the remaining refracts into another material. The stress wave refracted into polyurethane coating of NEA and EEA induced by the incident stress wave σ_I can be calculated by the following formulae [41],

$$\sigma_{T1} = \frac{2}{1+n_{M*S*}}\sigma_I \tag{7}$$

$$\sigma_{T3} = \frac{4}{(1+n_{M^*E^*})(1+n_{E^*S^*})}\sigma_I \tag{8}$$

where σ_{T1} and σ_{T3} are the stress waves refracted into polyurethane coating of NEA and EEA, $n_{M^*S^*} = (\rho C)_{M^*}/(\rho C)_{S^*}$, $n_{M^*E^*} = (\rho C)_{M^*}/(\rho C)_{E^*}$ and $n_{E^*S^*} = (\rho C)_{E^*}/(\rho C)_{S^*}$ are the impedance ratios of materials on both sides of the interface, where stress wave is refracted at NEA and EEA, ρ is the density of material, C is the velocity of stress wave.

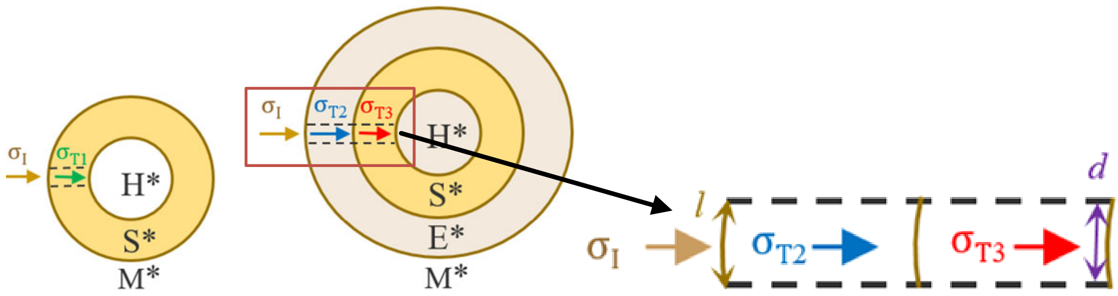

(a) (b) (c)

Fig. 8 Simplified analytical model of engineered aggregate

(a) NEA, (b) EEA, (c) Enlarged

In this study, the velocity of stress wave in matrix is calculated based on the response of NC specimen at elastic range, and the velocities of stress wave propagating in enhanced coating layer and polyurethane coating are calculated based on $C = \sqrt{E/\rho}$ [24]. Table 5 gives the impedances of different materials for EEA-steel-11.95 and NEA-11.79 in this study. Based on the impedances of different materials, it can be calculated that the stress wave refracted into polyurethane coating at NEA-11.79 is 2.68 times of that at EEA-steel-11.95, which indicates the steel enhanced coating layer can mitigate the stress wave refracting into polyurethane coating. Fig. 9 shows the strain time histories of polyurethane element E4 for NMC and EMC-steel specimens. The peak strain value of the polyurethane element for EEA-steel-11.95 is lower than that of NEA-11.79, but not substantially. It is because adding the steel enhanced coating layer can mitigate the stress wave refracting into polyurethane coating, which reduces the stress and strain of polyurethane coating. On the other hand, it causes less motion of heavy core, which leads to the increased deformation and stress of the polyurethane coating. Nonetheless, it should be noted that this simplification represents the true behaviour of EEA only when the loading and deformation of EEA is isotropic and uniform, i.e., EEA is under hydrodynamic load.

In reality, an EEA is not subjected to hydrodynamic load when 1D wave propagates insider a metaconcrete specimen. The results from simplified analytical derivation cannot be exactly compared to the numerical results based on 3D mesoscale model. Therefore, the analytical derivation here is used only to illustrate the wave transmission into different layers of an EEA.

Table 5 Impedance of different materials

Material	Density (kg/m^3)	Wave velocity (m/s)	Impedance (kg/m^{2}s)
Mortar matrix	2219	3846	8.54×10^6
Steel	7800	5064	3.95×10^7
Polyurethane (EEA-steel-11.95)	900	276	2.49×10^5
Polyurethane (NEA-11.79)	900	269	2.42×10^5

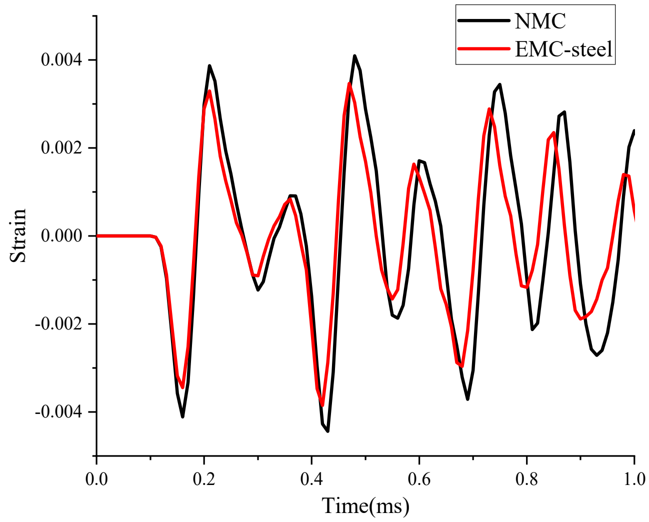

Fig. 9 Strain time histories of E4 (polyurethane element) for NMC specimen and EMC-steel specimen

Fig. 10 shows the stress time histories of E1 (a mortar element on the specimen periphery surface) as designated in Fig. 2 for different specimens. The first compressive stress peaks and the first tensile stress peaks of E1 for EMC specimens are similar to those for NMC specimen, but lower than those for NC specimen by around 17.83% and 22.41%, respectively. More importantly, the peak stress values for both NMC and EMC specimens decrease with the propagation of stress wave in these specimens, which is because wave propagates through more number of engineered aggregates and each of them absorbs certain amount of wave energy induced by impulsive load through local vibration of hard core.

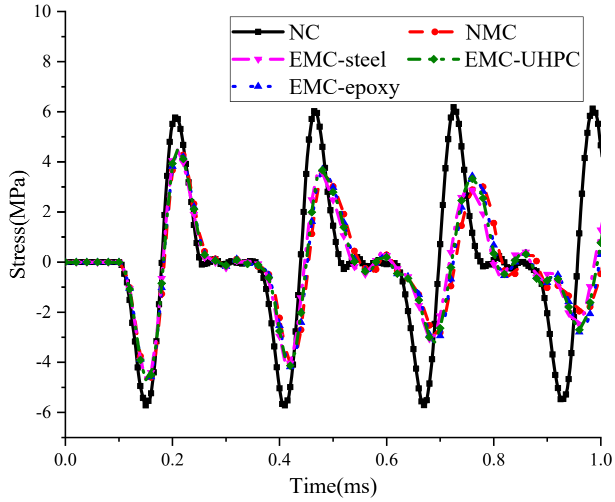

Fig. 10 Stress time histories of E1 (mortar element on the specimen periphery surface) for different specimens

4.2. Response of EMC specimen subjected to large impact loads

To study the effect of enhanced coating layer on the response of metaconcrete subjected to large impact loads, impulsive loads with 25 MPa and 50 MPa amplitudes as shown in Fig. 11 are applied to EMC specimens. The responses of NC and NMC specimens are also simulated for comparison. The inelastic response and material damage are also considered in the simulation. The simulation replicates spall test of concrete specimens.

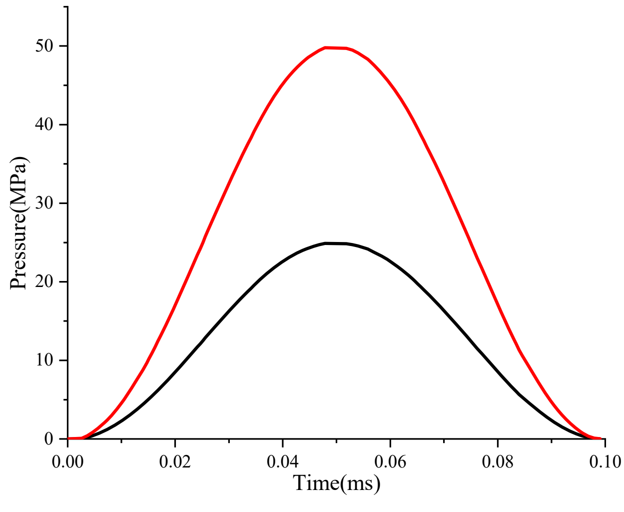

Fig. 11 Impulsive loads with 25 MPa and 50 MPa amplitudes and 0.1 ms duration

Fig. 12(a)-(e) show the damage patterns of NC, NMC and EMC specimens at $t = 2$ ms under the impulsive load with 25 MPa amplitude, respectively. The spall strength of concrete (σ) can be calculated by using Eq. (9), and the parameters used for calculation are given in Table 6.

$$\sigma = \frac{\rho C_0 \Delta V_{pb}}{2} \tag{9}$$

where ρ is the density of specimen, C_0 is the velocity of one-dimensional wave propagating in the specimen, and ΔV_{pb} is the pullback velocity recorded at the rear surface of the specimen. Fig. 13 shows the pullback velocity time histories of NC, NMC and EMC specimens.

As given in Table 6, EMC-steel specimen has the lowest pullback velocity, even lower than NMC specimen. This is probably because the steel enhanced coating layer has very different impedance from the mortar matrix, which affects the wave propagation in the specimen. However, as shown in Fig. 7, the amount of energy absorbed by the heavy core vibrations of EMC-steel is only slightly less than that of EEA with epoxy and UHPC coating, indicating EEA with an external steel layer is effective in mitigating wave energy although it affects the wave propagation velocity, which affects the enhancement of spall strength of EMC. Therefore, the enhanced coating layer should be properly designed with sufficient stiffness for not compromising the concrete material strength, and the impedance close to the mortar matrix to ensure smooth stress wave propagation. A too soft coating layer could lead to the reduced concrete strength while a too stiff coating layer affects stress wave propagation and transmission into the heavy core, which could reduce the energy absorption capacity of the EEA if the vibration of heavy core is not effectively excited.

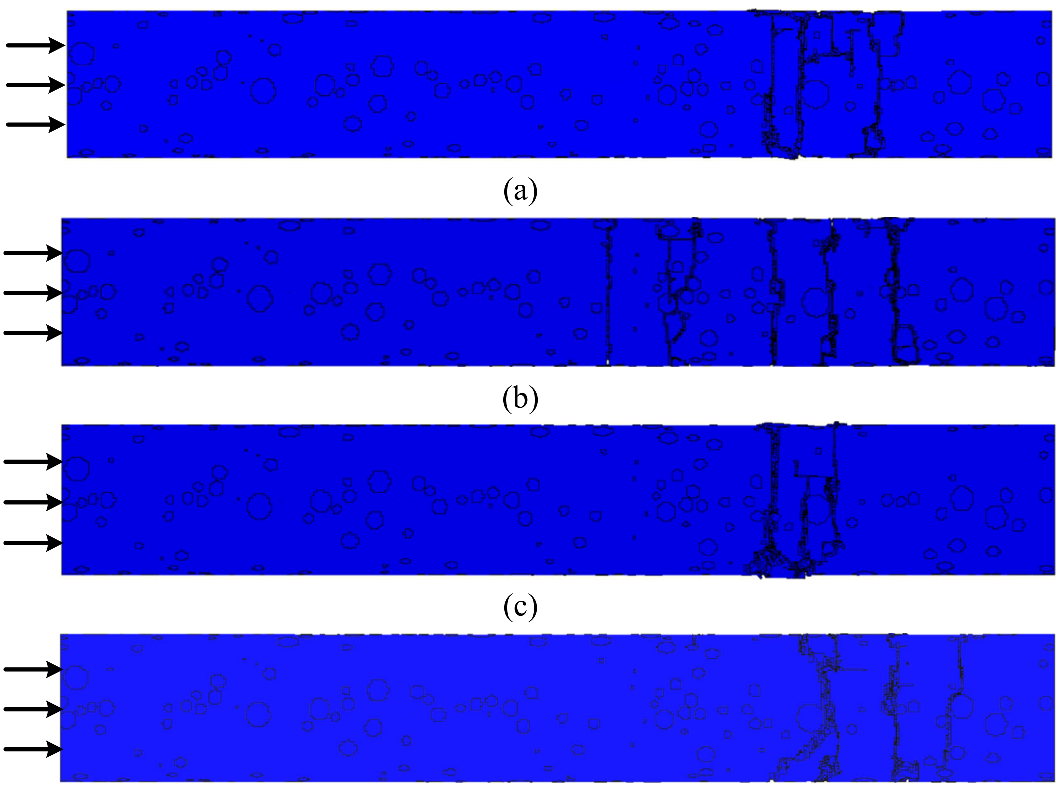

(a)

(b)

(c)

(d)

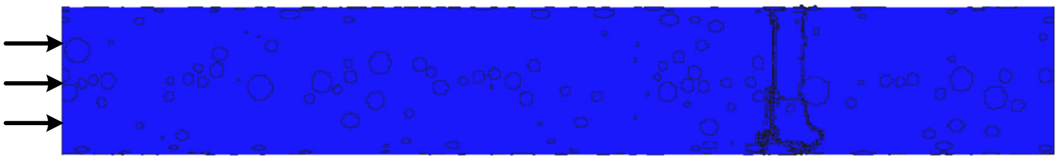

(e)

Fig. 12 Damage patterns of different specimens under impulsive load with 25 MPa amplitude (a) NC specimen, (b) NMC specimen (c) EMC-epoxy specimen, (d) EMC-steel specimen, (e) EMC-UHPC specimen

Table 6 Parameters used for calculating the spall strength of various metaconcrete specimens

Specimen	Density (kg/m^3)	Wave velocity (m/s)	Pullback velocity (m/s)	Spall strength (MPa)
NC	2219.8	3846.1	3.6	15.3
NMC	2214.2	3684.7	3.3	13.5
EMC-epoxy	2208.3	3703.7	3.9	15.9
EMC-steel	2380.8	3773.4	3.2	14.4
EMC-UHPC	2225.0	3703.6	3.9	16.1

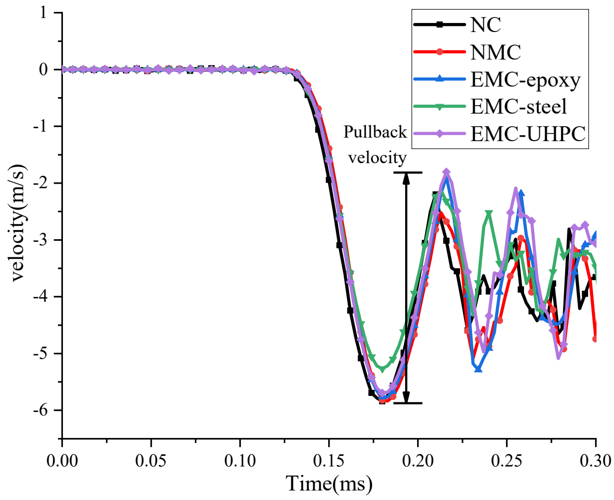

Fig. 13 Pullback velocity time histories for different specimens

As shown in Fig. 12, although NEA attenuates stress wave amplitude, as also observed in Jin et al. [24], NMC experiences more severe spall damage than NC because the added polyurethane coating reduces the concrete strength. The enhanced coating layer can improve the stiffness of interface between polyurethane coating and mortar matrix. The spall damage of EMC is less severe than that of NMC in general. In addition, the spall damage of EMC-epoxy and EMC-UHPC is less severe than that of NC. According to Eq. (9), the spall strength of EMC-epoxy, EMC-steel and EMC-UHPC is 17.8%, 6.7% and 19.3% higher than that of NMC. The spall strength of NMC is lower than that of NC by 11.8%. The spall strength of EMC-UHPC is slightly higher than that of NC, by 5.2%. It should be noted that damage to the mortar matrix before the resonance of EEA is effectively activated limits the enhancement of spall strength.

Fig. 14(a)-(e) show the damage patterns of NC, NMC and EMC specimens at t = 0.21 ms under the impulsive load with 50 MPa amplitude. The NMC specimen experiences compressive damage owing to the reduced concrete strength at the left side (as highlighted in red box), while NC and EMC specimens experience no compressive damage at the left side. It should be noted that although the amplitude of the applied impulsive load is higher than the mortar strength, mortar does not suffer compressive damage because of the strain rate effect that enhances the dynamic mortar strength. The compressive damage of NMC specimen is due to the relatively large deformation of mortar matrix induced by the low modulus of soft coating at NEA. The enhanced coating layer of EEA has higher stiffness than mortar and polyurethane, which enhances compressive strength of EMC specimen. Spalling damage occurs on the rear side of EMC specimens due to the reflection and superposition of stress wave. It is observed that the spall damage of EMC-epoxy and EMC-UHPC is less severe than that of NC. NMC specimen also experiences spall damage, but the damage level is less severe than that of NC and EMC specimens [22]. It is because the compressive damage at the left side of NMC specimen partially dissipates the wave energy.

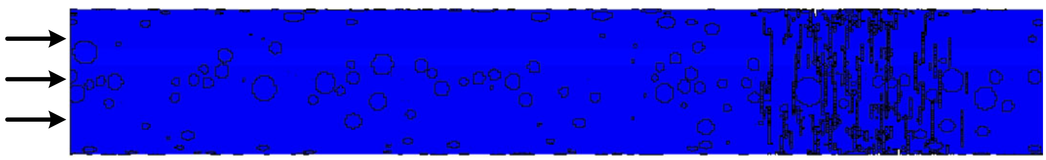

(a)

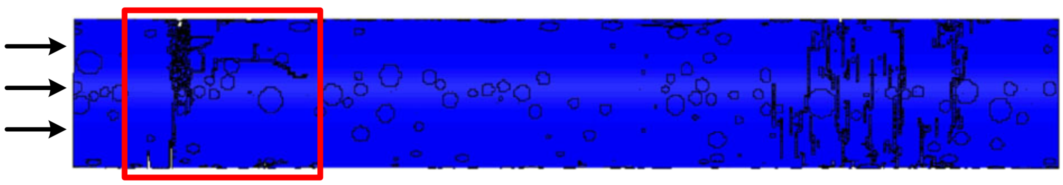

(b)

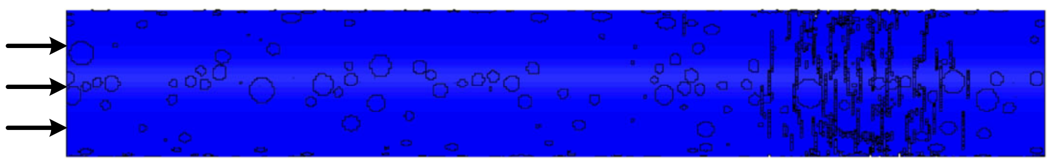

(c)

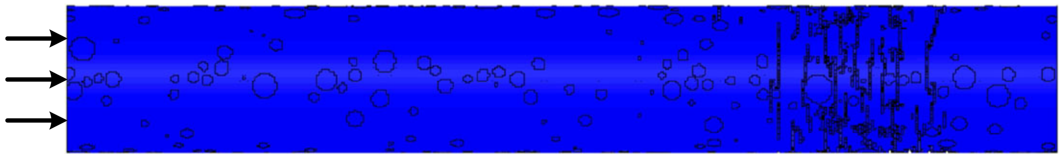

(d)

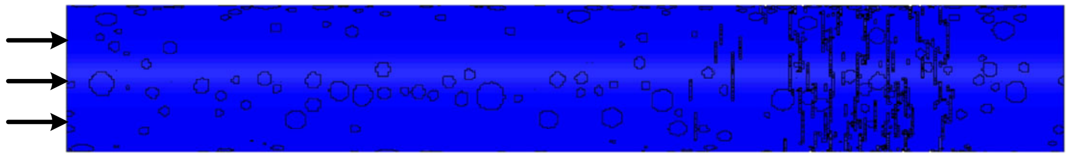

(e)

Fig. 14 Damage patterns of different specimens under impulsive load with 50 MPa amplitude (a) NC specimen, (b) NMC specimen, (c) EMC-epoxy specimen, (d) EMC-steel specimen, (e) EMC-UHPC specimen

These results demonstrate that adding an external stiff coating layer on NEA could effectively mitigate the problem of NEA on reducing the concrete strength, while still largely keep the functions of engineered aggregates on wave propagation mitigation through local vibrations of hard cores in engineered aggregates. Based on the results in this study, prototypes of enhanced engineered aggregates will be designed, fabricated and their performances will be tested in near future.

5. Conclusion

To overcome the shortcomings of the conventional engineered aggregate (NEA) in compromising the concrete strength, a new enhanced engineered aggregate (EEA) for metaconcrete is proposed in this study by adding an additional enhanced coating layer outside the conventional engineered aggregate. The EEA is designed via the software COMSOL to have its bandgap coincide with the predominant frequency of stress wave propagating in NC specimen. Three types of EEA aggregates with three enhanced coating layer materials (i.e., epoxy resin, steel, UHPC) are considered. A 3D meso-scale model of EMC specimen is established to predict the response of EMC in spall test via the software LS-DYNA. The effects of the enhanced coating layer on the bandgap characteristics of engineered aggregate are examined. The influences of adding enhanced coating layer on the energy absorption capacity, the wave attenuation characteristics and the spall strength of metaconcrete are also studied. The main conclusions are drawn below.

1. Adding an enhanced coating layer to the NEA slightly changes the bandgap properties of engineered aggregate. It slightly shifts the central bandgap frequency and narrows bandgap width.
2. Adding an enhanced coating layer to engineered aggregate overcomes the negative effect of NEA on concrete strength. It slightly reduces the energy absorption capacity of engineered aggregate, but the overall performances of EEA in energy absorption and mitigation of stress wave propagation are comparable to NEA while the strength of concrete mixed with EEA aggregates is not compromised.
3. With only about 2.59% of the total specimen volume replaced by engineered aggregates, the first peak compressive stress and the first peak tensile stress amplitude in concrete specimen mixed with NEA and EEA aggregates are reduced by around 17.83% and 22.41%, respectively, through local vibrations of hard cores of engineered aggregates as compared to those in NC specimen. More significant reductions are observed as stress wave propagates through more numbers of engineered aggregates in NMC and EMC specimens.
4. The spall strength of metaconcrete with NEA aggregates is lower than normal concrete, however, the spall strength of metaconcrete mixed with EEA aggregates are comparable or even slightly higher than normal concrete. Owing to the comparable concrete strength and mitigation of wave propagation, metaconcrete specimens with EEA aggregates experienced less severe spalling damage as compared to the normal concrete specimen.
5. The spall strength of EMC-epoxy, EMC-steel and EMC-UHPC is 17.8%, 6.7% and 19.3% higher than that of NMC, indicating UHPC is a better material for enhanced coating layer.

In summary, EMC with enhanced engineered aggregates can yield similar stress wave attenuation and has higher spall strength as compared to NMC. Enhanced engineered aggregates therefore can be used to mix metaconcrete to achieve the stress wave mitigation performance while not compromise the concrete strength as metaconcrete with conventional engineered aggregates.

6. Acknowledgement

The authors are grateful for the financial support from the Australian Research Council (ARC)

via Laureate Fellowship FL180100196.

Reference

[1] A.A. Delouei, A. Emamian, H. Sajjadi, M. Atashafrooz, Y. Li, L. Wang, D. Jing, G. Xie, A Comprehensive Review on Multi-Dimensional Heat Conduction of Multi-Layer and Composite Structures: Analytical Solutions, Journal of Thermal Science, 30 (2021) 1875-1907.

[2] A.A. Delouei, A. Emamian, S. Karimnejad, H. Sajjadi, A. Tarokh, On 2D asymmetric heat conduction in functionally graded cylindrical segments: A general exact solution, International Journal of Heat and Mass Transfer, 143 (2019) 118515.

[3] A.A. Delouei, A. Emaminan, S. Karimnejad, H. Sajjadi, A closed-form solution for axisymmetric conduction in a finite functionally graded cylinder, International Communications in Heat and Mass Transfer, 108 (2019) 104280.

[4] Y.H. Zhou, P.J. Wei, Y.Q. Li, Q.H. Tang, Continuum model of acoustic metamaterials with diatomic crystal lattice, Mechanics of Advanced Materials and Structures, 24 (2017) 1059-1073.

[5] Z.Y. Lin, Z.J. Wu, G.P. Zou, F.M. Li, C.Z. Zhang, A.J. Sun, Q. Du, Band-gap characteristics of elastic metamaterial plate with axial rod core by the finite element and spectral element hybrid method, Mechanics of Advanced Materials and Structures, (2021) 1-18.

[6] Y.T. Su, X. Wu, J. Shi, A novel 3D printable multimaterial auxetic metamaterial with reinforced structure: Improved stiffness and retained auxetic behavior, Mechanics of Advanced Materials and Structures, (2020) 1-11.

[7] X. Zhang, Z. Liu, Negative refraction of acoustic waves in two-dimensional phononic crystals, Applied Physics Letters, 85 (2004) 341-343.

[8] N. Fang, D. Xi, J. Xu, M. Ambati, W. Srituravanich, C. Sun, X. Zhang, Ultrasonic metamaterials with negative modulus, Nature Materials, 5 (2006) 452-456.

[9] Z.Y. Liu, X.X. Zhang, Y.W. Mao, Y. Zhu, Z.Y. Yang, C.T. Chan, P. Sheng, Locally resonant sonic materials, science, 289 (2000) 1734-1736.

[10] S.J. Mitchell, A. Pandolfi, M. Ortiz, Metaconcrete: designed aggregates to enhance dynamic performance, Journal of the Mechanics and Physics of Solids, 65 (2014) 69-81.

[11] H. Huang, C. Sun, G. Huang, On the negative effective mass density in acoustic metamaterials, International Journal of Engineering Science, 47 (2009) 610-617.

[12] Y. Shi, J. Wang, J. Cui, Experimental studies on fragments of reinforced concrete slabs

under close-in explosions, International Journal of Impact Engineering, (2020) 103630.
[13] Z.Y. Liu, C.T. Chan, P. Sheng, Three-component elastic wave band-gap material, Physical Review B, 65 (2002) 165116.
[14] Mahmoud. I. Hussein, Michael. J. Leamy, M. Ruzzene., Dynamics of Phononic Materials and Structures: Historical Origins, Recent Progress, and Future Outlook, Applied Mechanics Reviews, 66 (2014) 040802.
[15] J.K. Huang, Z.F. Shi, Application of Periodic Theory to Rows of Piles for Horizontal Vibration Attenuation, International Journal of Geomechanics, 13 (2013) 132-142.
[16] Z.Y. Liu, C.T. Chan, P. Sheng, Analytic model of phononic crystals with local resonances, Physical Review B, 71 (2005) 014103.
[17] J.C. Hsu, T.T. Wu, Lamb waves in binary locally resonant phononic plates with two-dimensional lattices, Applied Physics Letters, (2007).
[18] Z.B. Cheng, Z.F. Shi, Y.L. Mo, H.J. Xiang, Locally resonant periodic structures with low-frequency band gaps, Journal of Applied Physics, 114 (2013) 2022.
[19] S.J. Mitchell, A. Pandolfi, M. Ortiz, Investigation of elastic wave transmission in a metaconcrete slab, Mechanics of Materials, 91 (2015) 295-303.
[20] S.J. Mitchell, A. Pandolfi, M. Ortiz, Effect of brittle fracture in a metaconcrete slab under shock loading, Journal of Engineering Mechanics, 142 (2016) 04016010.
[21] C. Xu, W.S. Chen, H. Hao, The influence of design parameters of engineered aggregate in metaconcrete on bandgap region, Journal of the Mechanics and Physics of Solids, 103929 (2020).
[22] H.X. Jin, H. Hao, Y.F. Hao, W.S. Chen, Predicting the response of locally resonant concrete structure under blast load, Construction and Building Materials, 252 (2020).
[23] H.X. Jin, W.S. Chen, H. Hao, Y.F. Hao, Numerical study on impact resistance of metaconcrete (in Chinese), Science China (Physics, Mechanics & Astronomy), 49 (2019).
[24] H.X. Jin, H. Hao, W.S. Chen, C. Xu, Spall behaviors of metaconcrete: 3D meso-scale modelling, International Journal of Structural Stability and Dynamics, (2021) 2150121.
[25] G. Chen, Y.F. Hao, H. Hao, 3D meso-scale modelling of concrete material in spall tests, Materials and Structures, 48 (2015) 1887-1899.
[26] H.J. Wu, Q.M. Zhang, F.L. Huang, Q.K. Jin, Experimental and numerical investigation on

the dynamic tensile strength of concrete, International Journal of Impact Engineering, 32 (2005) 605-617.

[27] P.B. Xu, H. Xu, H.M. Wen, 3D meso-mechanical modeling of concrete spall tests, International Journal of Impact Engineering, 97 (2016) 46-56.

[28] L. Zhang, S.S. Hu, D.X. Chen, Z.Q. Yu, F. Liu, An Experimental Technique for Spalling of Concrete, Experimental Mechanics, 49 (2009) 523-532.

[29] A. Brara, F. Camborde, J.R. Klepaczko, C. Mariotti, Experimental and numerical study of concrete at high strain rates in tension, Mechanics of Materials, 33 (2001) 33-45.

[30] P. Wriggers, S.O. Moftah, Mesoscale models for concrete: Homogenisation and damage behaviour, Finite Elements in Analysis and Design, 42 (2006) 623-636.

[31] L.J. Malvar, J.E. Crawford, J.W. Wesevich, D. Simons, A plasticity concrete material model for DYNA3D, International Journal of Impact Engineering, 19 (1997) 847-873.

[32] Y.F. Hao, H. Hao, Numerical evaluation of the influence of aggregates on concrete compressive strength at high strain rate, International Journal of Protective Structures, 2 (2011) 177-206.

[33] C. DeArmitt, Magnetite, In: Palsule S. (eds) Polymers and Polymeric Composites: A Reference Series. S, Berlin, Heidelberg, 2016.

[34] Q. Su, H. Wu, H.S. Sun, Q. Fang, Experimental and numerical studies on dynamic behavior of reinforced UHPC panel under medium-range explosions, International Journal of Impact Engineering, 148 (2020) 103761.

[35] Y.F. Hao, H. Hao, X.H. Zhang, Numerical analysis of concrete material properties at high strain rate under direct tension, International journal of impact engineering, 39 (2012) 51-62.

[36] L. Malvar, J. Crawford, Dynamic increase factors for concrete. In: Twenty-eighth DDESB seminar, Orlando, Florida, (1998).

[37] Y.F. Hao, H. Hao, Numerical Investigation of the dynamic compressive behaviour of rock materials at high strain rate, Rock Mechanics and Rock Engineering, 46 (2013) 373-388.

[38] G.M. Ren, H. Wu, Q. Fang, J.Z. Liu, Effects of steel fiber content and type on dynamic compressive mechanical properties of UHPCC, Construction and Building Materials, 163 (2018) 826-839.

[39] H. Wu, G.M. Ren, Q. Fang, J.Z. Liu, Effects of steel fiber content and type on dynamic

tensile mechanical properties of UHPCC, Construction and Building Materials, 173 (2018) 251-261.

[40] W. Zhang, B. Xue, Elastic modulus adjustable polyurethane composition, scaffold composite and preparation method thereof, in, China, 2017.

[41] L. Wang, Foundations of stress waves, National Defense Industry Press (in Chinese), Beijing, 1985.